Development of a Sodar for the Study of Planetary Boundary Layer

By Yoshiki Ito, Shigeru Murabayashi and Yasushi Mitsuta

(Manuscript received December 10, 1984)

Abstract

A new sodar system is developed, which has capability of measuring three dimensional wind components in the planetary boundary layer with one parabolic reflector. This is realized by newly designed defocus feed horn arrangements, i.e. three speakers sharing one parabolic reflector make three acoustic beams independently. Wind components are deduced from Doppler frequency shifts with the complex covariance method. Wind data can be obtained up to 400 m in height with resolution of 40 m and intervals of 2.5 minutes by the present system.

1. Introduction

Remote sensing of planetary boundary layer by acoustic sounding technique was first achieved by McAllister of Australia in 1968[1]. He proved the backscattering signal from temperature fluctuations on a facsimile recorder. Scattering of sound from meteorological objects such as temperature or wind fluctuations is much larger than that of electro-magnetic wave, therefore remote sensing by sonic means has many advantages in short range measurements. Little[2] reviewed the possibilities of acoustic sounding techniques, and evaluated the system parameters required for these techniques. He concluded that the possible applications of the acoustic sounding technique are detection of 1) the vertical profile of wind speed and direction by using the Doppler method, 2) the vertical profile of humidity by using a multi-frequency system, 3) the location and intensity of temperature inversion, 4) the three-dimensional spectrum of temperature inhomogeneity, and 5) the three-dimensional spectrum of mechanical turbulence by using the bistatic mode system. His review stimulated both scientific and commercial developments of acoustic sounding system which was named as SODAR (SOund Detection And Ranging).

Typical research works concerning sodar are summarized in **Table 1**. Leading studies have been made by the research group of the Wave Propagation Laboratory of NOAA, USA. Beran and Clifford[26], for example, first succeeded in observing three dimensional wind velocity components by the three axis acoustic sounder with a Doppler system. Beran *et al.*[10] developed this system into a wind profile monitoring system for the airport without disturbing air traffic. Kaimal and Haugen[22] compared their sodar with tower mounted anemometers within the height range from 30 m to 150 m and found good agreement between their wind speed outputs.

Table 1 Summaries of sodars in the world. Some of the references are omitted here.

Name	Year	Carrier frequency (Hz)	Peak power (watt) (A): Acoustic (E): Electric	Pulse width (msec)	Receiver bandwidth (Hz)
McAllister, L.G. *et al.*[1]	1968	950	15 (A)	10	100
Wescott, J.W. *et al.*[3]	1970	2000	40 (E)	20～200	100
Fukushima, M. *et al.*[4]	1971	850	100 (E)	60	40
Cronenwett, W.T. *et al.*[5]	1972	1500	150 (E)	42.6	50
Shaw, N.A.	1974	1000	100 (E)	100	10
Bourne, I.A. *et al.*	1974	1350	2700* (E)	—	5
Aubry, M. *et al.*[6]	1974	2000	—	200	100
Balser, M. *et al.*[7]	1974	4500	40* (E)	60	—
Ottersten, H. *et al.*[8]	1974	2485	50 (E)	50, 100, 200	100
Kjelaas, A.G. *et al.*[9]	1974	1750～	10 (A)	100	100
Beran, D.W. *et al.*[10]	1974	1050*	800～1000**	100	100
Neff, W.D.[11]	1975	1750* 2250 2750	25, 100** (E)	6, 20, 30	100, 300
Owens, E.J.[12]	1975	2000 2500 3333	100 (E)	10～990	—
Mandics, P.A. and E.J. Owens[13]	1975	2000	100 (E)	50	30
Hall Jr., F.F., *et al.*[14]	1975	1750 1900 2150	—	40	—
Goroch, A.K.[15]	1976	1600	140 (E)	100	40
声雷送組[16]	1976	1588	—	100	40
Fukushima, M. *et al.*[17]	1976	930	100 (E)	60	40
Asimakopoulos, D.N. *et al.*[18]	1976	1730	25 (A)	74	50
Petersen, E.L. and N.O. Jensen	1976	1600	140 (E)	100	40
Shaw, N.A. *et al.*	1977	1350	2700* (E)	400	5
Arnold, L.N.[19]	1977	1286	21.6, 46.8 (E)	270	53
Nater, W. and H. Richner[20]	1977	1190	200 (E)	150	30
Mitsuta, Y. and Y. Ito[21]	1977	1600	83 (E)	54, 102, 236, 504	100
Kaimal, J.C. and D.A. Haugen[22]	1977	3600 3000	100* (E)	—	—
Balser, M. *et al.*	1977	2000 4000	150 (E)	160 80	—
Caughey, S.J. *et al.*[23]	1978	1732	—*	50	60
Hayashi, M. *et al.*[24]	1978	1600	100 (E)	50 100	100
von Gogh, R.G. and P. Zib[25]	1978	1600	140 (E)	100	40

Table 1 (continued)

Maximum gain (dB)	Pulse repetition period (sec)	Antenna diameter (m)	Half power beamwidth (deg)	Attenuation factor	Remarks
—	2	0.2*	—	—	*49 speakers
—	2∼10	1.5	8°	0.335×0.183	
—	3, 6, 12	16.	5°	—	
—	—	1.21	—	0.01	
—	20	1.5	12°	—	
—	0.4	1.5	—	—	*81 speakers
—	5.0	—	—	—	
—	1.0	1.8	—	—	*each of 10 drivers
—	3.0, 5.0	0.9	9°	—	ship mounted sodar
—	8.0	1.52	±5°	—	
—	—	3.0	—	—	one vertical T–R and two inclined T–R and two inclined R *1050 Hz and above two frequencies **four horns connected in series
—	—	1.52	±5°	0.045 0.045 0.28	*multi- or single-frequency **multi: 25, single: 100
162	1, 2, 4, 8	—	—	—	
—	2.0	1.2	10°	—	ship mounted sodar
—	—	—	—	—	
—	7	—	—	—	Aerovironment Model 300
—	3, 4, 6	1.5	8°	—	
—	6	0.62×2	10°	—	
—	2.3	0.165*	—	0.029	*36 speakers
—	7	—	—	—	Aerovironment Model 300
—	—	1.5	—	—	*81 speakers
—	3.94	1.6	—	—	balloonborne sodar
—	6	1.5	—	—	
157	4.3, 10.7 8.5, 21.3	1.8	8°	0.096	
—	2.0	1.2	—	—	each of three horns connected in series *fan-beam transmitter, pencil-beam receiver
—	5.0 2.5	1.2 0.9	—	—	Xonics
—	2	—*	—	—	*36 speakers
—	8, 16	1.2	—	—	
—	7	—	—	—	Aerovironment Model 300

The existence of the sharp discontinuity of temperature or the region of strong thermal disturbances in the atmosphere can also be detected by a sodar. von Gogh and Zib[25] compared the height of sodar echoes with radiosonde observations and concluded that heights of stratified echoes are consistent with heights of the bases of stable layers aloft, in 45 cases out of 58 stratified echo cases. However, their quantitative analyses of received return signal intensities were not so successful. For unknown reasons, the estimated turbulent intensities of temperature and wind velocity by acoustic means were not in good agreement with in-situ measurements.

Recent efforts on the sodar have been focused on developing it as an all weather and multi-purpose boundary layer remote sensor. Hardesty *et al.*[27] have constructed a hybrid boundary layer wind sensor, which is essentially a sodar but becomes a Doppler radar in case of rain when reception of acoustic return signal is impeded. An attempt to develop a system capable of simultaneous measurements of wind and temperature is the Radio Acoustic Sounding System (RASS) by Frankel *et al.*[28], which is the technique of Doppler-tracking of an acoustic pulse by an electromagnetic radar.

The study and development of the sodar in Kyoto University was started in 1970. The first test equipment with a 9 speaker system was constructed in 1972 and the improved system with a parabolic reflector in 1977[21]. The third generation with Doppler analyser has been completed recently, which is shown in the present paper.

2. Principle of sodar observation

2.1 Acoustic reflection and scattering in the atmosphere

An acoustic wave propagates straight in a uniform and homogeneous medium. However, when it reaches the discontinuity surface of the medium, a part of the acoustic energy is reflected and the rest is refracted into the other side of the surface, and, when it passes through a turbulent region, a portion of the energy is also scattered. Sodar is the system which finds out acoustic refractive index discontinuities or disturbances in the atmosphere by detecting the reflected or scattered signal of the transmitted acoustic signal.

The received signal intensity, P_r can be related to the transmitted power, P_t by the radar equation,

$$P_r = P_t E_t E_r e^{-2\alpha R} q , \tag{1}$$

where q is the received fraction of the acoustic reflection from the scattering volume, E_t and E_r the efficiencies in power of the transmitter and receiver respectively, α the acoustic attenuation coefficient and R being the range. q is determined by the characteristics of the object, α depends on the physical condition of the medium, and the others are the characteristic parameters of the sodar.

In the case of reflection caused by a discontinuity plane in the atmosphere,

q is related to acoustic reflectivity, Q_r by the following relation

$$q = \left(\frac{r}{R\Theta}\right)^2 Q_r , \tag{2}$$

where r is the radius of parabolic reflector and Θ being the acoustic beam width.

Acoustic reflectivity, Q_r of the atmospheric discontinuity surface can be written as follows[29].

$$Q_r = \left(\frac{\lambda\, \Delta n}{4\pi h}\right)^2 , \tag{3}$$

where λ is the wavelength of the acoustic signal, Δn the difference in the index of refraction and h being the depth of the transitional layer. The depth of the transitional layer in the boundary layer is not clear and is one of the subjects to be studied, however, but it can be very thin for stably stratified layer comparable to the wavelength of the acoustic signal. If we assume discontinuity, Δn is nearly equal to $\Delta T/2T_0$, where ΔT is the temperature difference and T_0 being the average temperature.

Equation (3) becomes

$$Q_{ra} = \left(\frac{\lambda}{4\pi h}\cdot\frac{\Delta T}{2T_0}\right)^2 \approx 2\times 10^{-8}\left(\frac{\lambda}{h}\right)^2 \Delta T^2 . \tag{4}$$

Therefore, as we can easily construct a sodar sensitive enough to detect reflectivity of 10^{-12} at a distance of a few hundred meters, the temperature discontinuity of tenths of degree can be detected if the thickness of transitional layer is thin enough.

While the reflectivity of electro-magnetic waves can also be evaluated by Eq. (2). The reflectivity of electro-magnetic waves, Q_{re} at the temperature discontinuity becomes[30]

$$Q_{re} = \left\{\frac{\lambda}{4\pi h}\left(7.8\times 10^{-5}\,\frac{p\Delta T}{T_0^2}\right)\right\}^2 \approx 6\times 10^{-15}\left(\frac{\lambda}{h}\right)^2 \Delta T^2 . \tag{5}$$

where p is air pressure. Thus acoustic reflectivity is about seven orders larger than that of an electro-magnetic wave. This is one of the great advantages of remote sensing by acoustic means.

Return signals are also obtained for scattering from the turbulent region in the atmosphere. The scattered power of the acoustic waves from the turbulent region of the refractive index is represented as follows[2],

$$\sigma_a(\theta) = 0.016\, k^{1/3} \cos^2\theta\, C_{na}^2 \sin^{-11/3}\left(\frac{\theta}{2}\right), \tag{6}$$

$$C_{na}^2 = 1.84\,\frac{C_v^2}{C^2}\cos^2\frac{\theta}{2} + \frac{C_T^2}{(2T)^2}, \tag{7}$$

where $\sigma_a(\theta)$ is acoustic scattering cross section per unit volume and unit solid angle at the scattering angle of θ, k the wave number (1/m), T and C being the mean values of temperature and acoustic velocity in the scattering volume, and C_{na}^2, C_v^2, and C_T^2 are the structure constants for acoustic refractive index, wind velocity and air temperature respectively. In this treatment, the humidity fluctuation and the correlation between wind and air temperature fluctuations are neglected. k is normally chosen to fall within the inertial subrange of the atmospheric turbulence.

The backscattering cross section per unit volume and unit solid angle can be obtained by replacing π for θ in equations (6) and (7)

$$\sigma(\pi) = 0.004\, k^{1/3}\, C_T^2/T^2\,. \tag{8}$$

As is clear from this equation, no contribution of wind fluctuation is expected for the pure backscattering of sound.

Fig. 1 shows an example of the dependence of temperature structure function, C_T^2 on height under conditions of free convection[31]. From this figure, we can expect C_T^2 to be 10^{-5} deg^{2}cm$^{-2/3}$ at the height of 1000 m in the free convection case, and this corresponds to acoustic reflectivity of the order of 10^{-11} for wavelength of a usual acoustic sounder. This is detectable reflectivity for the usual sodar, which means we can expect that return signals are detectable for most of the sodar from the whole space of unstable stratification.

The contribution of wind fluctuation upon acoustic scattering increases rapidly

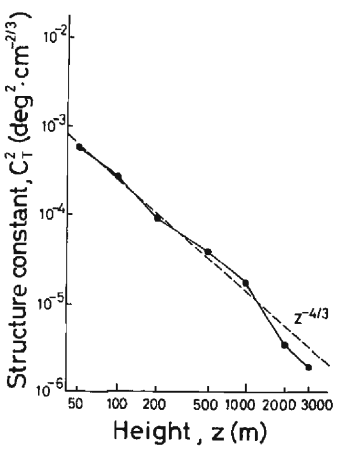

Fig. 1 An example of the dependence of the structure constant of temperature fluctuations C_T^2 on height under conditions of free convection (after Tatarskii, V.I.[31])

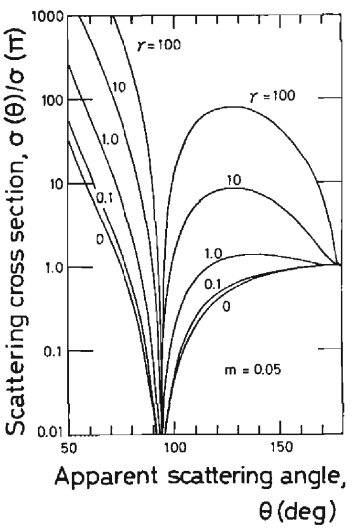

Fig. 2 Scattering cross section as a function of apparent scattering angle with ratio m of mean wind to speed of sound and $\gamma = C_v^2 T^2/C_T^2 C^2$ as parameters (after Brown, E.H.[32])

with decreasing scattering angle from 180°. The scattering cross section $\sigma(\theta)$ as a function of scattering angle θ is shown in **Fig. 2**[32]. In this figure $\sigma(\theta)$ is shown in the form of the ratio to the backscattering cross section of temperature fluctuations $\sigma(\pi)$, as $\sigma(\theta)/\sigma(\pi)$. The parameter $\gamma=(C_v^2T^2/C_T^2C^2)$ represents the contribution of wind fluctuations in the scattered signal. Taking the value of γ as 10, a typical value in the unstable lower troposphere, the scattering cross section for 110° to 150° becomes almost an order of magnitude larger than that for backscattering only by temperature fluctuations. Thus we can expect enough strong return signals from wind turbulences for a bistatic sodar of inclined mode.

The received return signal intensity, P_r of scattering from turbulent region can be written as follows reforming Eq. (1),

$$P_r = \frac{C\tau_p}{2}\sigma(\theta)\, P_t E_t E_r\, e^{-2\alpha R}\frac{AG}{R^2}, \tag{9}$$

where τ_p is the pulse length, A the antenna aperture, G an effective aperture factor. The parameters except C, $\sigma(\theta)$, α and R are the characteristic values for the hardware of the sodar. Therefore, reflectivity can be computed from this equation by determining P_r and R from the sodar record assuming attenuation of sound in the air, α.

The attenuation of sound in the air measured by Harris[33] in the test chamber is as shown in **Fig. 3**. It shows that the absorption of sound at the frequency of 2 kHz will amount to about 1.1 dB/100 m at relative humidity above 40% and at air temperature of 15°C and about 4.2 dB/100 m in the vicinity of 15% at 6°C. This relation has been confirmed by Aubry *et al.*[34] in field experiments. As is clear from this figure, precise estimation of humidity and air temperature are required in the quantitative analysis of return signal intensity.

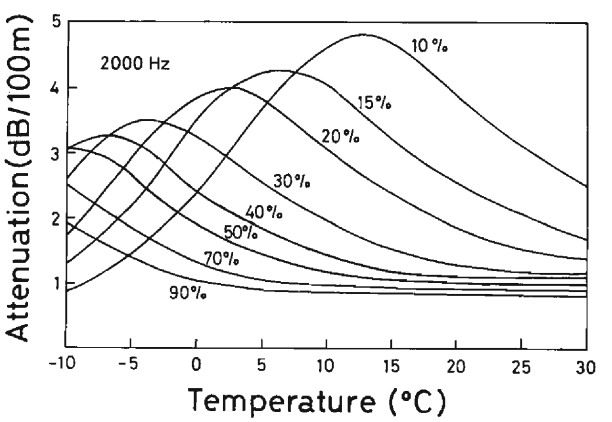

Fig. 3 Attenuation of sound in air versus temperature for various values of relative humidity (after Harris, C.M.[33])

2.2 Doppler wind measurement

Wind velocity, the movement of reflecting or scattering volume of the sound, can be detected from the Doppler shift of the returned signal. Schematic diagram of remote sensing of wind by acoustic means is shown in **Figs. 4** and **5**. **Fig. 4** is called as the three axis bistatic mode and **Fig. 5** as the three axis monostatic mode sodar. The bistatic sodar employs two inclined transmitters or receivers, which have fan beams to radiate for the whole height range, and a vertically directed transmitter-receiver with a pencil beam. The bistatic mode has the advantages of 1) the contribution of wind fluctuations to the scattered signal can be expected, and 2) the scattering volume is apparently the same for three axis beams. The monostatic sodar consists of three transmitter-receivers with pencil beams which measure the radial wind component for each sensor. The monostatic mode is characterized by 1) the small area which is enough for antenna installation, and 2) the sensi-

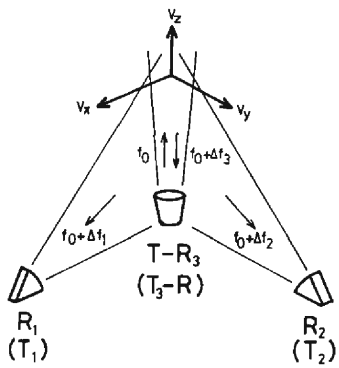

Fig. 4 Three axis bistatic mode sodar

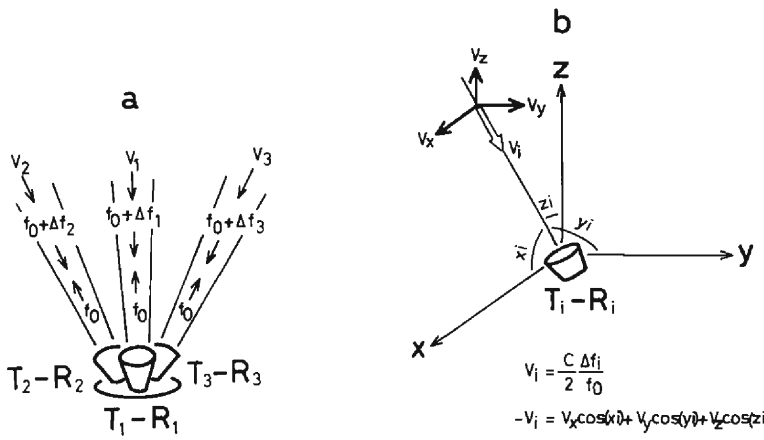

Fig. 5 Three axis monostatic mode sodar.
a: Antenna arrangement.
b: Principle of Doppler wind measurement.

tivity to the horizontal wind is the same for the whole height range. The antenna arrangement, either bistatic or monostatic mode, should be selected according to the purpose of observation.

Doppler shift, Δf of the backscattered return signal from the scattering volume moving with velocity component, V in the beam direction is shown as follows,

$$V = \frac{C}{2}\frac{\Delta f}{f_0}, \tag{10}$$

where V is measured towards the receiver and f_0 is the frequency of the original signal.

In the case of the three axis monostatic mode sodar as shown in **Fig. 5**, three components of wind velocity (V_1, V_2 and V_3) in the directions of three beams can be related to the three components of wind in Cartesian coordinate (V_x, V_y and V_z), where V_x is east-west component measured with positive eastward, V_y north-south component with positive northward and V_z vertical component with positive upward, as follows.

Assuming homogeneity of wind in the sampling volume considered, the formula becomes,

$$-\begin{pmatrix} V_1 \\ V_2 \\ V_3 \end{pmatrix} = \boldsymbol{A}\begin{pmatrix} V_x \\ V_y \\ V_z \end{pmatrix},$$

where

$$\boldsymbol{A} = \begin{pmatrix} \cos(x1) & \cos(y1) & \cos(z1) \\ \cos(x2) & \cos(y2) & \cos(z2) \\ \cos(x3) & \cos(y3) & \cos(z3) \end{pmatrix}, \tag{11}$$

and $\cos(xi)$, $\cos(yi)$, and $\cos(zi)$ ($i=1, 2, 3$) being direction cosines of i-th beam axis relative to x-, y-, z-axises. Solving Eq. (11)

$$\begin{pmatrix} V_x \\ V_y \\ V_z \end{pmatrix} = -\boldsymbol{A}^{-1}\begin{pmatrix} V_1 \\ V_2 \\ V_3 \end{pmatrix}. \tag{12}$$

Therefore, V_x, V_y, and V_z can be obtained from V_1, V_2, and V_3. And V_1, V_2 and V_3 are calculated from the Doppler frequency shift of each monostatic component of the sodar by Eq. (10).

2.3 Techniques of Doppler frequency estimation

There are several ways to obtain the Doppler frequency shifts of received signals. In the case of sodar application, the following methods are employed; 1)

Wave count, a method to count the time duration between zero crossings of received signal, which is the simplest method but applicable only in good signal to noise ratio conditions, 2) Phase Locked Loop (PLL), a method to control the Voltage Controlled Oscillator (VCO) output so as to track the frequency of returned signal by feedback, 3) Filter bank, a bank of narrow band filters with center frequencies, 4) Fast Fourier Transform (FFT), a method to obtain the spectrum by fast Fourier transformation technique by a microcomputer, 5) Complex covariance, a method to calculate the complex covariance function from in-phase and quadrature components of received signal to obtain the first and second moments of a spectral density function.

Among above methods, 3) through 5) are regarded as excellent ones from the standpoint of noise immunities. 3) is too large to handle in hardware. 4) is characterized by flexibility in Doppler frequency deduction because the full spectrum is calculated, while 5) the complex covariance method gives the first and second moments immediately and is not biased by the white noise. The principle and observed examples based on the complex covariance method are described in the following.

The principle of measurements by the complex covariance method is, as stated above, to obtain the first and second moments of spectrum, which are equivalent to the mean frequencies and variances of received signals, respectively. This is an application of the pulse pair processing techniques in a Doppler radar.

The k-th moment of non-negative integrable function $S(f)$ is defined by

$$\mu_k(S) = \frac{\int_{-\infty}^{\infty} f^k S(f)\, df}{\int_{-\infty}^{\infty} S(f)\, df}. \tag{13}$$

Therefore the mean frequency, $\bar{f}$, that is the first moment of the spectral density, $S(f)$, becomes

$$\mu_1(S) = \bar{f} = \frac{\int_{-\infty}^{\infty} f S(f)\, df}{\int_{-\infty}^{\infty} S(f)\, df}. \tag{14}$$

Since the spectral density and the covariance function $R(\tau)$ constitute a Fourier transform pair,

$$R(\tau) = \int_{-\infty}^{\infty} S(f)\, e^{i2\pi f\tau}\, df. \tag{15}$$

Expressing (14) in terms of $R(\tau)$

$$\mu_1(S) = \frac{1}{i2\pi} \frac{\dot{R}(0)}{R(0)}, \tag{16}$$

where $\dot{R}(0)$ is the derivative of $R(\tau)$ at $\tau=0$. The second moment that represents the spread of spectral density can be expressed in the same manner.

The covariance function is written in polar form as

$$R(\tau) = A(\tau)\, e^{i2\pi\phi(\tau)}\,, \tag{17}$$

substituting (17) into (16)

$$\mu_1(S) = \dot{\phi}(0)\,. \tag{18}$$

For small $\tau \neq 0$,

$$\mu_1(S) \approx \frac{\phi(\tau)}{\tau}\,. \tag{19}$$

For the symmetric power spectrum, as the function $\phi(\tau)$ is a linear function of τ, the mean frequency estimate is not biased[35], therefore Eq. (19) becomes an equality, and

$$\mu_1(S) = \frac{1}{2\pi\tau}\tan^{-1}\frac{\mathrm{Im}\,[R(\tau)]}{\mathrm{Re}\,[R(\tau)]}\,. \tag{20}$$

Thus the mean frequency can be expressed in terms of the real and imaginary parts of the complex covariance function.

Fig. 6 indicates the block diagram of the data processing in the homodyne covariance method. As seen in this figure, the angular frequency ω' of received signal is first mixed by a reference clock signal of transmitting frequency ω_0 and a reference phase-shifted 90°, respectively, then through low pass filters, so we can get the in-phase X_r and the quadrature X_i components of a Doppler frequency $\omega=(\omega'-\omega_0)$. The complex sample $Z(n)$ can be obtained by sampling these signals with a proper sampling duration τ as **Fig. 7**.

$$Z(n) = X_r(n) + i\, X_i(n)\,. \tag{21}$$

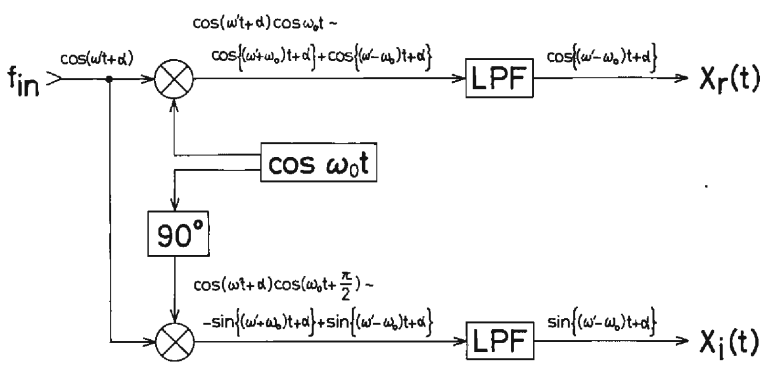

Fig. 6 Block diagram of analog circuit to generate complex signals

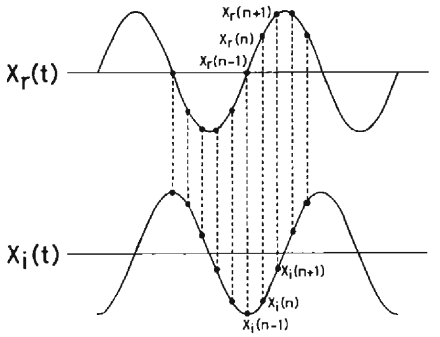

Fig. 7 Sampling chart of complex signals

Since the covariance function is given by

$$R(\tau) \approx \frac{1}{N-1} \sum_{n=1}^{N-1} Z(n)\, Z^*(n+1)\,, \tag{22}$$

from Eq. (20), we obtain the Doppler frequency of received signal $\bar{f}$ as

$$\bar{f} = \frac{1}{2\pi\tau} \tan^{-1} \frac{\mathrm{Im}\,[\overline{Z(n)\, Z^*(n+1)}]}{\mathrm{Re}\,[\overline{Z(n)\, Z^*(n+1)}]}\,. \tag{23}$$

Real and imaginary parts of $\overline{Z(n)Z^*(n+1)}$ are expressed as

$$\mathrm{Re}\,[\overline{Z(n)\, Z^*(n+1)}] = \frac{1}{N-1} \sum_{n=1}^{N-1} \{X_r(n)\, X_r(n+1) + X_i(n)\, X_i(n+1)\}\,, \tag{24}$$

$$\mathrm{Im}\,[\overline{Z(n)\, Z^*(n+1)}] = \frac{1}{N-1} \sum_{n=1}^{N-1} \{-X_r(n)\, X_i(n+1) + X_r(n+1)\, X_i(n)\}\,. \tag{25}$$

With Eqs. (23), (24), and (25) we can calculate Doppler frequency by at least two pairs of complex samples. However, in order to minimize the variance of such estimates, several dozens of sampling are needed.

The proper selection of a sampling duration τ depends on the unknown frequency spreading of the received signal and also on the signal to noise ratio[36]. Several to ten samplings per period of expected frequency are actually adopted in a Doppler sodar. In practical application, there are no problems on the bias caused by asymmetry of received spectra. Moreover the compensation of noise process would appear quite useful in a Doppler sodar application. Hence Eq. (20) becomes

$$\bar{f} = \frac{1}{2\pi\tau} \tan^{-1} \frac{\mathrm{Im}\,[R(\tau)] - \mathrm{Im}\,[R_n(\tau)]}{\mathrm{Re}\,[R(\tau)] - \mathrm{Re}\,[R_n(\tau)]}\,, \tag{26}$$

where $R_n(\tau)$ indicates the complex covariance of noise process.

3. The New Sodar System

3.1 Outline of the system

The specifications of the new system of the Disaster Prevention Research Institute, Kyoto University developed by the present authors are listed in **Table 2**, and is essentially almost the same as the previous system[21]. The functional block diagram of the system is shown in **Fig. 8**. This system is characterized by the new compact size antenna array and the new real time processor. The antenna has three transducers crossing 120° in azimuth on one reflector to make three axis monostatic beams, and the microcomputer carried out the Doppler wind deduction by the homodyne complex covariance method, which can be performed by a small computer.

As shown in **Fig. 8**, the carrier signal generated by an oscillator is provided to the gate and modulated to the pulsed carrier, and then fed into the transducer through the power amplifier. Acoustic pulses are transmitted from three transducers in every repetition interval in turn and returned signals are received by the same transducer. Received signals are led into the amplifier through the distance gain controller and then divided into the mixers and the detector. The mixers generate in-phase and quadrature component signals for Dŏppler analysis and the detector gives the signal intensity.

The individual components shown in **Fig. 8** are as follows. Oscillator is a quartz controlled oscillator with rectangular wave, whose accuracy is better than 10^{-5} at normal temperature. Dividers consist of CMOS-IC counters to make the carrier frequency, 1600 or 3200 Hz, and reference clocks for the mixers and also work as other timing generator. Gate produces the pulsed carrier signal and controls the pulse repetition interval of 3, 5 or 10 sec, and the pulse duration of 50, 100 or 250 msec, according to timing signal from the divider. Band Pass Filter is an active filter to form sine wave and Power Amplifier is the pushpull audio frequency amplifier unit with electric output of 10, 50, 100 or 300 watts. T-R switch protects the receiver from high voltage at the time of transmission by switching three

Table 2 System parameters of the new sodar system

Antenna array	3 axis monostatic with one reflector
Carrier frequency (f_0)	1600*, 3200 Hz
Output power (electric)	10, 50, 100*, 300 watts
Pulse duration	50, 100*, 250 msec
Pulse repetition period	3, 5, 10* sec
Parabolic reflector	
diameter	180 cm
Receiver	
gain (max)	150 dB
bandwidth	$\pm 10\%$ around f_0

* used in normal operation

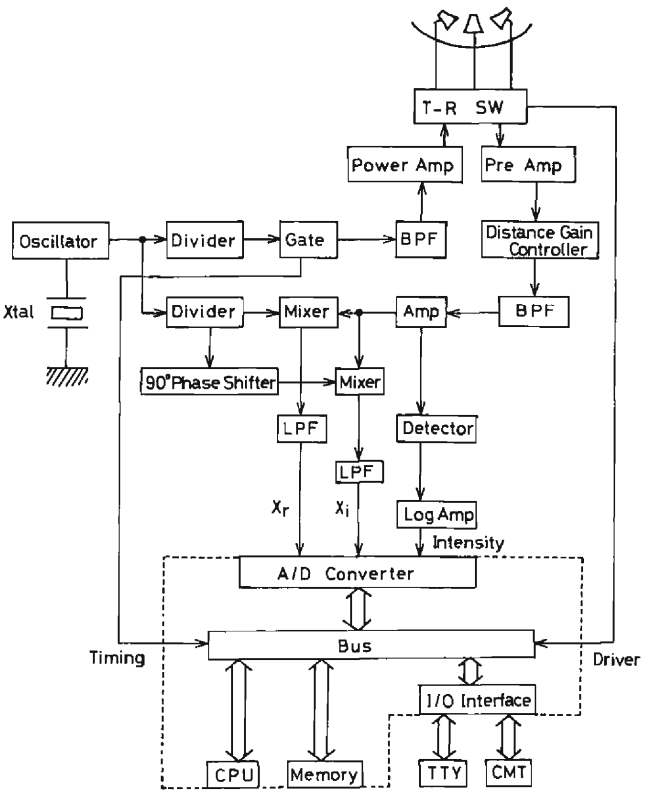

Fig. 8 Block diagram of the new sodar system

transducers in turn every repetition interval with mercury relays. Transducer and Reflector are the combination of three horn speakers and a parabolic reflector as shown in **Photo 1**. The horn speakers with defocus feed are placed to cross each other at 120° in the horizontal plane with a zenith angle of 20°. The reflector, which has a diameter of 180 cm, focal length of 58 cm, is surrounded by a sound absorbing wall of four meters high to reduce sidelobes and to prevent environmental noises. Distance Gain Controller compensates a round trip loss of acoustic signal caused by spherical expansion of a wave front and absorption in the atmosphere. The system gain increases with time after transmission of the sound pulse, not so far as to saturate the amplifier. Band Pass Filter is a precision active filter performing frequency response of about 75 dB/oct to discriminate the return signal from ambient noises. The bandwidth is $\pm 10\%$ around the carrier frequency, which keeps enough allowance for Doppler frequency shifts. Pre-Amplifier and Amplifier are high gain, low noise, low drift hybrid and FET operational amplifiers with total maximum gain of up to 150 dB. Mixers, Phase Shifter and Low Pass Filter work as a pre-processor for Doppler wind estimation to produce in-phase and quadrature components of the received signal. They are composed of multipliers,

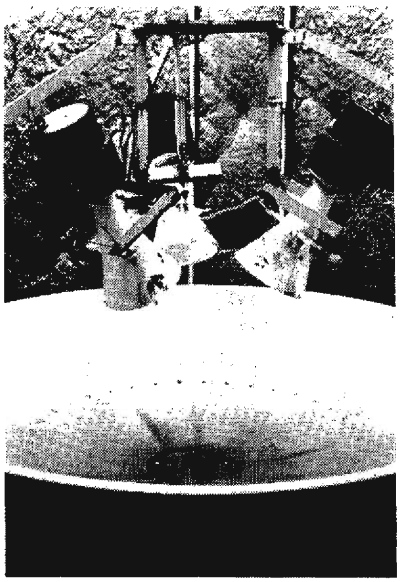

Photo 1 3 transducers with horn fixed above the parabolic reflector

active filters and others. Log Amplifier output, rectified by Detector, gives the signal intensity. Microcomputer equipped with 8-bit CPU, 64 kB Memories, Analog to Digital Converter and other peripherals are used to calculate the Doppler frequency shift and wind velocity, the results of computation are recorded on Cassette Magnetic Tape.

3.2 Performance test of components

An experimental test of the transmitter and receiver was made to prove the system performance. **Photo 1** shows the arrangement of horn drivers inside of the antenna. This arrangement, so called defocus feed horn, was designed to have a defocusing angle of about 20°, producing a beam with zenith angle of 16°. The antenna radiation pattern was tested. When the driver unit is on the axis of the parabolic reflector, it is found that the acoustic source is approximately to located at the horn aperture. Fixing the horn drivers at the calculated positions, we meas-

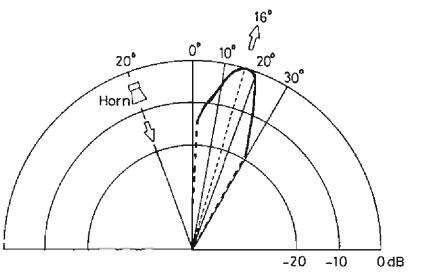

Fig. 9 Transmitting gain pattern actually measured in the radial section

ured the radiation pattern in acoustic farfield, outside of the range of about D^2/λ, where D is the diameter if a circular plane surface source is assumed and λ is the wave length.

The beam pattern in the radial section obtained by the preceding method is shown in **Fig. 9**. As seen in this figure, the beam direction is 16° from the zenith and the beam width is about 13° at 1600 Hz. Theoretical radiation pattern of this reflector for the circular plane surface source on the focus shows a beam width of about 8°. The beam width of the present system is a little broader than that in normal use, however, considering the defocus feed with three drivers and a reflector combination, such a broader beam is inevitable. By such a beam, it is able to measure scattering volume, for instance of about 70 meters in horizontal and 20 meters in altitude at the height of 300 meters.

Test of the Doppler frequency analysis system was carried out by emitting acoustic signals. The mono-frequency signal produced by a sine wave generator was fed into an antenna with background noises. For various signal frequency and intensity, the output values were compared with those of the original signal.

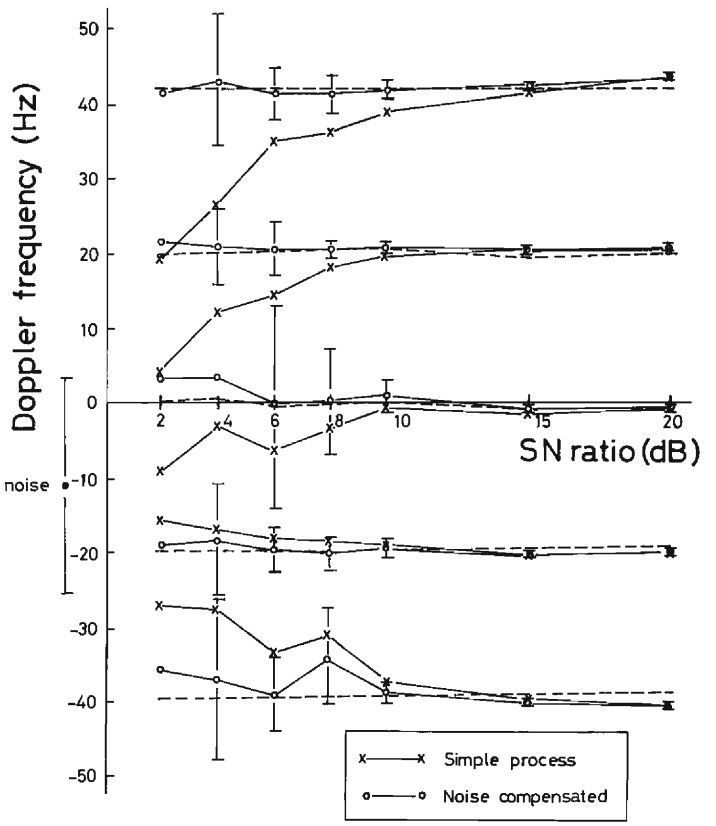

Fig. 10 Test results of Doppler frequency deduction by the complex covariance method

Since the receiver collects both the signals and background noises, we can find out the dependence of the results on a signal to noise ratio. The results are shown in **Fig. 10**. As seen in this figure, the variance of the frequency estimation shown by the long T mark increases with decreasing of the signal to noise ratio. And the variance is relatively large when the Doppler shift is zero. The mean frequency estimations based on the simple process are biased by the background noise shown in the left side of the figure at lower signal to noise ratios, but the one based on the noise compensation process mentioned in Eq. (26) gives the proper value down to about 4 dB. Hence the noise compensation process has recognized to be useful for Doppler frequency estimation of the sodar, and has been adopted in the present system.

3.3 Details of data analysis

As shown in **Fig. 8**, the received signal frequency is beaten down to the Doppler components by the homodyne method, that is the received signal and the oscillator signals of 1.6 kHz (3.2 kHz) of in phase and 90° delayed in phase are mixed and detected, producing the two output signals, X_r and X_i in Eq. (21), which are fed into the A–D converter of the data processing system.

The sampling interval, τ and the total sample number N in Eq. (22) are selected to be 0.002 sec and more than 60 from experiments as shown in the previous section. Therefore the signal are digitized at the rate of 500 Hz for 10 sec of pulse repetition interval and the covariance functions are computed for every 120 sampling of the data. The background noise covariance is detected just before the pulse transmission in 10 sec intervals. The covariances are computed by Eqs. (24) and (25). The Doppler shift can be computed with noise compensation by Eq. (26). The same covariance for the noise process, $R_n(\tau)$ computed from the noise just before the signal transmission is used throughout one cycle of the signal analysis.

Thus three wind components (V_i) for every 40 m height intervals are computed succesively in 30 sec or 3 cycles of repetition. The data of four soundings for each component are averaged and the wind velocity data set is computed. The total time to obtain one data set including the data processing time is 2 min 30 sec.

The computation of three components of wind velocity in Cartesian coordinate in X(E–W), Y(N–S) and Z directions are made from the three components of wind, V_i $(=C\Delta f_i/2f_0)$ $(i=1, 2, 3)$ by Eq. (12), postulating wind homogeneity in the beam spreading volume. Practical form of Eq. (12) is determined by the actual values of direction cosines, cos (xi), cos (yi), and cos $z(i)$. **Fig. 11** shows an example of obtaining cos (xi) from the azimuth angle α_i, measured from y-axis clockwise, and the zenith angle zi of the i-th beam axis. It is simply expressed,

$$\cos(xi) = \sin(zi)\sin\alpha_i\,, \quad (i = 1, 2, 3)\,. \tag{27}$$

And similarly,

$$\cos(yi) = \sin(zi)\cos\alpha_i\,, \quad (i = 1, 2, 3)\,. \tag{28}$$

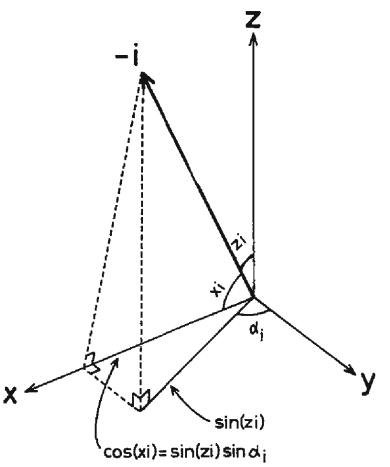

Fig. 11 An example to deduce direction cosines in Eq. (11). $\mathbf{i}$ is the unit vector toward the ith acoustic beam axis. α_i is the azimuth angle of the i-th acoustic beam axis measured from y-axis (northward) clockwise.

In the present system, three acoustic beams are radiated to cross at 120° in horizontal, with zenith angle of 16°, and the beam-1 is directed northward. Therefore, $z1=z2=z3=16°$, and $\alpha_1=0°$, $\alpha_2=120°$, $\alpha_3=240°$. Then direction cosines are calculated by Eqs. (27) and (28) and the matrix becomes,

$$\boldsymbol{A}=\begin{pmatrix} 0 & \sin 16° & \cos 16° \\ \sin 16°\sin 120° & \sin 16°\cos 120° & \cos 16° \\ \sin 16°\sin 240° & \sin 16°\cos 240° & \cos 16° \end{pmatrix}. \tag{29}$$

And with calculation for obtaining inverse matrix of $\boldsymbol{A}$, each component of wind velocity is obtained by,

$$V_x = -2.09\,V_2+2.09\,V_3\,, \tag{30}$$

$$V_y = -2.42\,V_1+1.21\,V_2+1.21\,V_3\,, \tag{31}$$

$$V_z = -0.347\,V_1-0.347\,V_2-0.347\,V_3\,. \tag{32}$$

Thus the wind data averaged over the space volume of about 100 m in the horizontal and 40 m in the vertical dimension and over 2.5 min are obtained from the present system. The results are recorded on a cassette magnetic tape in digital form.

The maximum detectable height in the field measurement is about 400 m in good condition and it decreases but is observable to a certain extent even in moderately noisy conditions such as drizzle. However, the pulsive noise from an aircraft or a bird inables the observation.

4. Concluding remarks

A newly designed three dimensional Doppler sodar system has been developed. The defocused antenna system was specially designed for the present system in order to decrease the total volume of the antenna system, which usually needs three transducers and reflectors. One large parabolic reflector is used to produce three directional signals by three transducers. The arrangement of the three transducers was decided by computer simulation to give the most effective radiation patterns. Although the beamwidth becomes a little broader, the system can measure wind velocity up to 400 m in height with a resolution of 40 m. The Doppler frequency shift deduction is made by the homodyne complex covariance method using a small 8-bit CPU with slower A/D converter. Owing to these efforts, the new system is compact and easy to handle in practical observations. This system was first used in field observation in the late summer of 1981, the results of which will be reported in another paper[37].

Acknowledgments

The authors would like to express their appreciation to Kaijo Denki Co. Ltd. for their hearty cooperation in designing and developing the present sodar system. This work was partly supported by Grant-in-Aid from the Ministry of Education, 484007 and 00502017.

References

1) McAllister, L.G., J.R. Pollard, A.R. Mahoney and P.J.R. Shaw: Acoustic Sounding —A New Approach to the Study of Atmospheric Structure, Proc. IEEE, Vol. 57, No. 4, 1969, pp. 579–587.
2) Little, C.G.: Acoustic Methods for the Remote Probing of the Lower Atmosphere, Proc. IEEE, Vol. 57, No. 4, 1969, pp. 571–578.
3) Wescott, J.W., W.R. Simmons and C.G. Little: Acoustic Echo-sounding Measurements of Temperature and Wind Fluctuations, ESSA Technical Memorandum, ERTM-WPL5, 1970, pp. 24.
4) Fukushima, M., K. Akita and I. Kasuya: Experiments on the Lower Troposphere Using an Acoustic Sounder, Rev. Radio Res. Lab. Jap., Vol. 17, 1971, pp. 401-406 (in Japanese).
5) Cronenwett, W.T., G.B. Walker and R.L. Inman: Acoustic Sounding of Meteorological Phenomena in the Planetary Boundary Layer, J. Appl. Meteor., Vol. 11, 1972, pp. 1351–1358.
6) Aubry, M., R. Chezlemas and A. Spizzichino: Preliminary Results of the Atmospheric Acoustic Sounding Program at CNET, Bound.-Layer Meteor., Vol. 7, 1974, pp. 513–519.
7) Balser, M., C.A. McNary and A.E. Nagy: Acoustic Backscatter Radar System for Tracking Aircraft Trailing Vortices, J. Aircraft, Vol. 11, 1974, pp. 556–562.
8) Ottersten, H., M. Hurtig, G. Stilke, B. Brümmer and G. Peters: Shipborne Sodar Measurements During Jonswap 2, J. Geophys. Res., Vol. 79, 1974, pp. 5573–5584.
9) Kjelaas, A.G., D.W. Beran, W.H. Hooke and B.R. Bean: Waves Observed in the Planetary Boundary Layer Using an Array of Acoustic Sounders, J. Atmos. Sci., Vol. 31, 1974, pp. 2040–2045.
10) Beran, D.W., B.C. Willmarth, F.C. Carsey and F.F. Hall, Jr.: An Acoustic Doppler Wind Measuring System, J. Acoust. Soc. Am., Vol. 55, 1974, pp. 334–338.
11) Neff, W.D.: Quantitative Evaluation of Acoustic Echoes from the Planetary Boundary Layer,

NOAA Tech. Rep., ERL-322-WPL 38, 1975, pp. 34.
12) Owens, E.J.: NOAA Mark VII Acoustic Echo Sounder, NOAA Tech. Mem., ERL WPL-12, 1975, pp. 71.
13) Mandics, P.A. and E.J. Owens: Observations of the Marine Atmosphere Using a Ship-Mounted Acoustic Sounder, J. Appl. Meteor., Vol. 14, 1975, pp. 1110–1117.
14) Hall Jr., F.F., J.G. Edinger and W.D. Neff: Convective Plumes in the Planetary Boundary Layer, Investigated with an Acoustic Echo Sounder, J. Appl. Meteor., Vol. 14, 1975, pp. 513–523.
15) Goroch, A.K.: Comparison of Radiosonde and Acoustic Echo Sounder Measurements of Atmospheric Thermal Strata, J. Appl. Meteor., Vol. 15, 1976, pp. 520–521.
16) 大気物理研究所声雷送組：単点声雷送与境界層大気探測，中国科学院大気物理研究所報，1976, pp. 42–54.
17) Fukushima, M., K. Akita, Y. Masuda and H. Tanaka: Features of Sodar Echoes Observed at Miyakojima Island during the AMTEX '75, J. Radio Res. Lab., Vol. 23, 1976, pp. 235–246.
18) Asimakopoulos, D.N., R.S. Cole, S.J. Caughey and B.A. Crease: A Quantitative Comparison between Acoustic Sounder Returns and the Direct Measurement of Atmospheric Temperature Fluctuations, Bound.-Layer Meteor., Vol. 10, 1976, pp. 137–147.
19) Arnold, L.N.: A Balloonborne Acoustic Sounder, J. Appl. Meteor., Vol. 16, 1977, pp. 971–982.
20) Nater, W. and H. Richner: Thermal Plumes Detected by an Acoustic Echo Sounder, J. Appl. Meteor., Vol. 16, 1977, pp. 986–989.
21) Mitsuta, Y. and Y. Ito: Measurement of Planetary Boundary Layer by the Acoustic Sounder, Annuals Disast. Prev. Res. Inst., Kyoto Univ., No. 20 B–1, 1977, pp. 157–172 (in Japanese).
22) Kaimal, J.C. and D.A. Haugen: An Acoustic Doppler Sounder for Measuring Wind Profiles in the Lower Boundary Layer, J. Appl. Meteor., Vol. 16, 1977, pp. 1298–1305.
23) Caughey, S.J., B.A. Crease, D.N. Asimakopoulos and R.S. Cole: Quantitative Bistatic Acoustic Sounding of the Atmospheric Boundary Layer, Quart. J.R. Met. Soc., Vol. 104, 1978, pp. 147–161.
24) Hayashi, M., O. Yokoyama and Y. Kobori: Acoustic Doppler Measurements of Vertical Velocity in the Atmosphere, J. Met. Soc. Japan, Vol. 56, 1978, pp. 516–522.
25) von Gogh, R.G. and P. Zib: Comparison of Simultaneous Tethered Balloon and Monostatic Acoustic Sounder Records of the Statically Stable Lower Atmosphere, J. Appl. Meteor., Vol. 17, 1978, pp. 34–39.
26) Beran, D.W. and S.F. Clifford: Acoustic Doppler Measurements of the Total Wind Vector, AMS Second Symp. on Meteor. Observ. Instru., Mar. 1972, pp. 100–110.
27) Hardesty, R.M., P.A. Mandics, D.W. Beran, and R.G. Strauch: The Dulles Airport Acoustic-Microwave Radar Wind and Wind Shear Measuring System, Bull. Amer. Meteor. Soc., Vol. 58, No. 9, 1977, pp. 910–918.
28) Frankel, M.S., N.J.F. Chang and M.J. Sanders, Jr.: A High-Frequency Radio Acoustic Sounder for Remote Measurement of Atmospheric Winds and Temperature, Bull. Amer. Meteor. Soc., Vol. 58, No. 9, 1977, pp. 928–934.
29) Hall Jr., F.F., and W.D. Neff: Comments on "A Mesoscale Phenomenon Revealed by an Acoustic Sounder", J. Appl. Meteor., Vol. 16, 1977, pp. 109–111.
30) Ottersten, H., K.R. Hardy and C.G. Little: Radar and Sodar Probing of Waves and Turbulence in Statically Stable Clear-Air Layers, Bound.-Layer Meteor., Vol. 4, 1973, pp. 47–89.
31) Tatarskii, V.I.: The Effects of the Turbulent Atmosphere on Wave Propagation, Israel Program for Scientific Translations. 1971, pp. 472.
32) Brown, E.H.: Some Recent NOAA Theoretical Work on Echo Sounding in the Atmosphere, J. Geophys. Res., Vol. 79, No. 36, 1974, pp. 5567–5571.
33) Harris, C.M.: Absorption of Sound in Air versus Humidity and Temperature, J. Acoust. Soc. Am., Vol. 40, 1966, pp. 148–159.
34) Aubry, M., F. Bandin, A. Weill and P. Rainteau: Measurement of the Total Attenuation of Acoustic Waves in Turbulent Atmosphere, J. Geophys. Res., Vol. 79, 1974, pp. 5598–5606.
35) Sirmans, D. and B. Bumgarner: Numerical Comparison of Five Mean Frequency Estimators, J. Appl. Meteor., Vol. 14, 1975, pp. 991–1003.
36) Miller, K.S. and M.M. Rochwarger: A Covariance Approach to Spectral Moment Estimation, IEEE Trans. Inform. Theory, IT-18, 1972, pp. 588–596.
37) Mitsuta, Y. and S. Uchida: Convective Motion in the Cumulus Sub-Cloud Layer, J. Climate Appl. Meteor., Vol. 24, 1985 (to be published).